JOURNAL OF Materials CHEMISTRY

Chemical deposition of PbS on a series of ω-functionalised self-assembled monolayers

Fiona C. Meldrum,*[a] Johannes Flath[b] and Wolfgang Knoll[b]

[a]*Department of Chemistry, Queen Mary and Westfield College, University of London, London E1 4NS. E-mail: F.C.Meldrum@qmw.ac.uk*
[b]*Max-Planck-Institut für Polymerforschung, Ackermannweg 10, D-55128, Mainz, Germany*

Received 11th September 1998, Accepted 23rd December 1998

Thin films of PbS were chemically deposited on a range of surfaces comprising self-assembled monolayers (SAMs) on Au and on the gold substrate itself. The influence of the monolayer terminal group on crystal growth was investigated, and a range of contrasting functionalities were employed: COOH, OH, NH_2, SO_3H and CH_3. The kinetics of film growth was measured using surface plasmon spectroscopy, and the structure of the films was studied by scanning electron microscopy and transmission electron microscopy. The orientation of the crystals in the films was studied by electron diffraction for very thin films and by X-ray diffraction for thicker films. The experiments demonstrated that both the gold substrate and the SAM terminal group were effective in influencing the nucleation and growth rates of the PbS films, the size of deposited crystals and the final orientation of crystals in the films. The composition of the deposition solution was also demonstrated to have a marked effect on the final orientation of the crystals.

Introduction

Numerous methods have been investigated which lead to the production of inorganic thin films on substrates. The uses are varied, with the inorganic films exhibiting, for example, selected optical, magnetic or ferroelectric properties, or acting as impermeable, hard and active coatings for sensors and smart material composites.[1–3] Control of the material properties is defined by the size, morphology and orientation of the constituent particles, and on the presence of defects. In turn, the structure of the film is determined by the material deposited, the preparation technique and the nature of the substrate itself.[4,5] Preparation methods can be classified as to whether they are performed in the gas or liquid phase. Gas-phase techniques such as Molecular Beam Epitaxy (MBE) and Chemical Vapour Deposition (CVD) are technologically demanding and are used to generate high quality films.[6–8] Wet chemical methods offer experimentally straightforward alternatives that do not require high temperatures or vacuum conditions. Traditional methods include Chemical Solution Deposition,[9–13] Electrochemical Deposition[14–16] and Successive Ionic Layer Adsorption and Reaction (SILAR).[17–19] Recently, much interest has been concentrated on the construction of thin films from pre-prepared particles *via* incorporation in polyelectrolyte layers,[20–22] adsorption on to functionally correspondent Self-Assembled Monolayers (SAMs),[23–25] transfer of close-packed monolayers of particles by the Langmuir–Blodgett (LB) technique,[26,27] and facile condensation on to substrates.[28,29] However, the majority of the latter methods result in a low density of particles and offer no control over particle orientation.

We here investigate the chemical deposition of PbS on a range of SAMs comprising terminally functionalised thiols on gold. Chemical deposition is a traditional method for preparing thin films of the metal chalcogenides. However, many questions remain regarding the mechanism involved. PbS was deposited on SAMs in order to investigate the influence of the expressed endgroup on the structure and orientation of the film produced and on the rate of PbS deposition. SAMs offer a very simple and flexible method to produce an organic interface of selected surface chemistry *via* modification of the monolayer terminal group,[30,31] and importantly can easily be patterned to achieve, for example, organised adsorption of cells or to direct crystal growth on to designated areas of the substrate.[32–34] A number of studies have been carried out where SAMs have provided substrates for crystal deposition[35–44] and data presented have suggested that SAMs can influence the nucleation density, crystal phase and the orientation of developing crystals.[42,44–48]

The present work represents an extension of earlier studies in which PbS was deposited on monolayers of 16-sulfanylhexadecanoic acid on Gold.[35] It was demonstrated that the kinetics of film deposition could be measured using Surface Plasmon Spectroscopy (SPS) and that these data could be correlated with the structural evolution of the film at various stages of deposition, as determined by Scanning Electron Microscopy (SEM) and Transmission Electron Microscopy (TEM). Studies of PbS deposition on SAMs patterned with areas of hydrophilic and hydrophobic functionalised thiols resulted in crystal growth on the hydrophilic areas only,[49] and showed that the monolayer terminal group was important in defining the product of crystal growth. We here investigate further the influence of the substrate on film formation by depositing PbS on SAMs bearing a range of contrasting endgroups: COOH, SO_3H, NH_2, OH, CH_3 and clean Au. The investigation also provides further information on the mechanism of chemical deposition.

Experimental

PbS was deposited on a range of Au/thiol self-assembled monolayers exhibiting contrasting terminal groups. The kinetics of crystal deposition was determined using Surface Plasmon Resonance, SPR, and the structure of the films was investigated by SEM and TEM. Detailed descriptions of the protocols involved have been given previously.[35]

Preparation of substrates

Gold films of thickness approximately 40 nm were evaporated on to LASFN9 glass slides (Hellma) which had been rigorously cleaned immediately prior to use. The evaporated films were then annealed at 250 °C for 3 h under cover on a hot plate, in order to increase the average size of the gold crystals.[35,50,51] All surfaces were covered with aluminium foil during heating to create the clean environment necessary to producing high quality films. After cooling the slides on the hot plate they

were immersed in a thiol solution, and self-assembly was allowed to proceed overnight, under argon. Immediately prior to use, the substrates were washed in a flow of ethanol for several minutes and dried with nitrogen gas. They were then mounted in cuvettes for surface plasmon analysis.

Self-assembled monolayers

A range of long-chain and short-chain thiol surfactants were investigated: 3-sulfanylpropanesulfonic acid, 3-sulfanylpropionic acid and dodecane-1-thiol (all obtained from Aldrich and used without further purification), 11-sulfanylundecanol (Fluka), 16-sulfanylhexadecanoic acid (synthesized as in ref. 52) and bis-aminododecyl-S, $H_2N(CH_2)_{12}S–S(CH_2)_{12}NH_2$, (synthesized as in ref. 53). All thiol surfactants were dissolved in ethanol to a concentration of 5×10^{-4} M, and stored under argon.

PbS Deposition

PbS films were prepared by a chemical deposition method. A solution of concentration 0.01 M $Pb(ClO_4)_2$, either 0.25 or 0.1 M NaOH, and thiourea concentration 0.2, 0.1, 0.05, 0.02, 0.01 or 0.005 M was prepared. Stock solutions of 0.1M $Pb(ClO_4)_2$, 2 or 5 M NaOH respectively, and freshly prepared thiourea of concentrations 0.4, 0.2, 0.1, 0.04, 0.05 and 0.05 M for the former concentrations were used. The $Pb(ClO_4)_2$ solution was diluted to the appropriate value, the NaOH solution added, and finally combined with the thiourea solution immediately prior to injection into the sample cuvette.

Surface plasmon spectroscopy (SPS)

Samples were mounted in Teflon cuvettes in the Kretschmann configuration using an LASFN9 prism to permit measurement against water and ethanol, and irradiation was from a 5 mW He–Ne laser, $\lambda=632.8$ nm.[35] Attenuated total reflection (ATR) at the prism/metal interface produces an evanescent field which excites surface plasmons in the metal film on momentum matching. The resonance curve is measured by recording the reflected light intensity as a function of incident angle, with excitement of the surface plasmon corresponding to the intensity minimum. The position of the minimum and shape of the curve vary as a function of the environment of the metal film.[54–56] Deposition of a thin film on the metal film results in a displacement of the curve corresponding to the optical thickness of the thin film, from which a geometric thickness can be derived on definition of the refractive index of the film. The experimental curves were analysed using fitting routines based upon the Fresnel equations for transmission and reflection of general multilayer assemblies. Resonance curves were calculated for a given set of conditions and compared with the experimental situation.

SPS Analysis of self-assembled monolayers

The thicknesses of the self-assembled monolayers formed on the gold substrates were measured using SPS.[54,57,58] A freshly evaporated gold substrate was mounted in a cuvette in the SPS spectrometer and resonance curves were measured against air and against ethanol. The ethanol was then removed and a portion of the thiol solution injected into the cuvette. A self-assembled film was allowed to form overnight, and the plasmon resonance curve then measured against the original thiol solution and after washing the cuvette through with about 50 ml ethanol. Analysis of the curves, assuming a film refractive index of $n=1.5$[58] yielded the film thickness, and an average over 4–5 measurements was taken. The values obtained were consistent with data in the literature and demonstrated the formation of complete monolayers.

SPS Measurement of the kinetics of PbS deposition

Plasmon resonance curves were measured of the prepared Au/SAM substrates against air and against water. The kinetics of deposition was then followed by monitoring the change in measured intensity at a fixed angle to the left of the resonance minimum (in the linear portion of the curve), typically at about 56°. The incident laser intensity was reduced to 25 nW using filters to prevent catalysis of crystal growth at the area of irradiation. The deposition solution was then injected into the cuvette and the change in intensity with time recorded.[35,54,58,59]

X-Ray diffraction

All PbS/Au/glass samples and the Au/glass substrates prior and subsequent to heating were analysed in reflection mode using a Phillips Guinier PW 1710 Diffractometer, operated using a cobalt source ($K\alpha$ $\lambda=1.78896$ Å).

Transmission electron microscopy

The structure of the PbS films deposited was studied at early stages of formation by TEM, using a JEOL 2000EX electron microscope operating at 200 kV or a Hitachi 1700 electron microscope operating at 100 kV. Specimens were then prepared for microscopy by separating the gold film supporting the deposited PbS crystals from the glass slide; the gold film was floated from the glass on to HF solution and transferred to 400 mesh copper TEM grids as described in detail elsewhere.[35,50,51]

Scanning electron microscopy

SEM was used to study the morphology of thicker PbS films. Specimens were cut to size and mounted on sample stubs. They were examined without further coating either in a Cambridge 360 SEM fitted with a LaB_6 filament, or in a Hitachi S-4500 Field-Emission SEM.

Results

For the sake of brevity, thiourea will be abbreviated to TU, and the stock solutions prepared with the 2 and 5 M NaOH will be termed 2 and 5 M solutions respectively. The SAMs will be referred to as: sulfonic (3-sulfanylpropanesulfonic acid), propionic (3-sulfanylpropionic acid), methyl (dodecane-1-thiol), alcohol (11-sulfanylundecanol), long-chain carboxyl (16-sulfanylhexadecanoic acid), and amine (bis-aminododecyl-S).

Kinetics of deposition

The deposition of PbS on the SAM/Au substrates was monitored with time using surface plasmon resonance, as has been described previously.[35] Briefly, the reflected intensity is measured for a fixed laser incidence angle over the period of film growth. The resonance condition of the gold film is altered on deposition of PbS, and the concomitant change in reflected intensity measured. Growth of PbS on the SAM produces an initial rapid increase in the intensity, followed by oscillations in the intensity as the film thickness increases. Measurement of the entire SPR curves over the course of deposition and subsequent fitting enables the shift in the resonance curves, and thus the reflected intensity at a given angle, to be correlated with the optical thickness of the deposited PbS film. These data can then be used to determine the deposited film thickness as a function of time.[54]

The kinetics data for the range of substrates and using the 2 and 5 M NaOH solutions are shown in Fig. 1. Some variation in measurements does occur between repetitions of identical samples, as is typical for the chemical deposition method, so

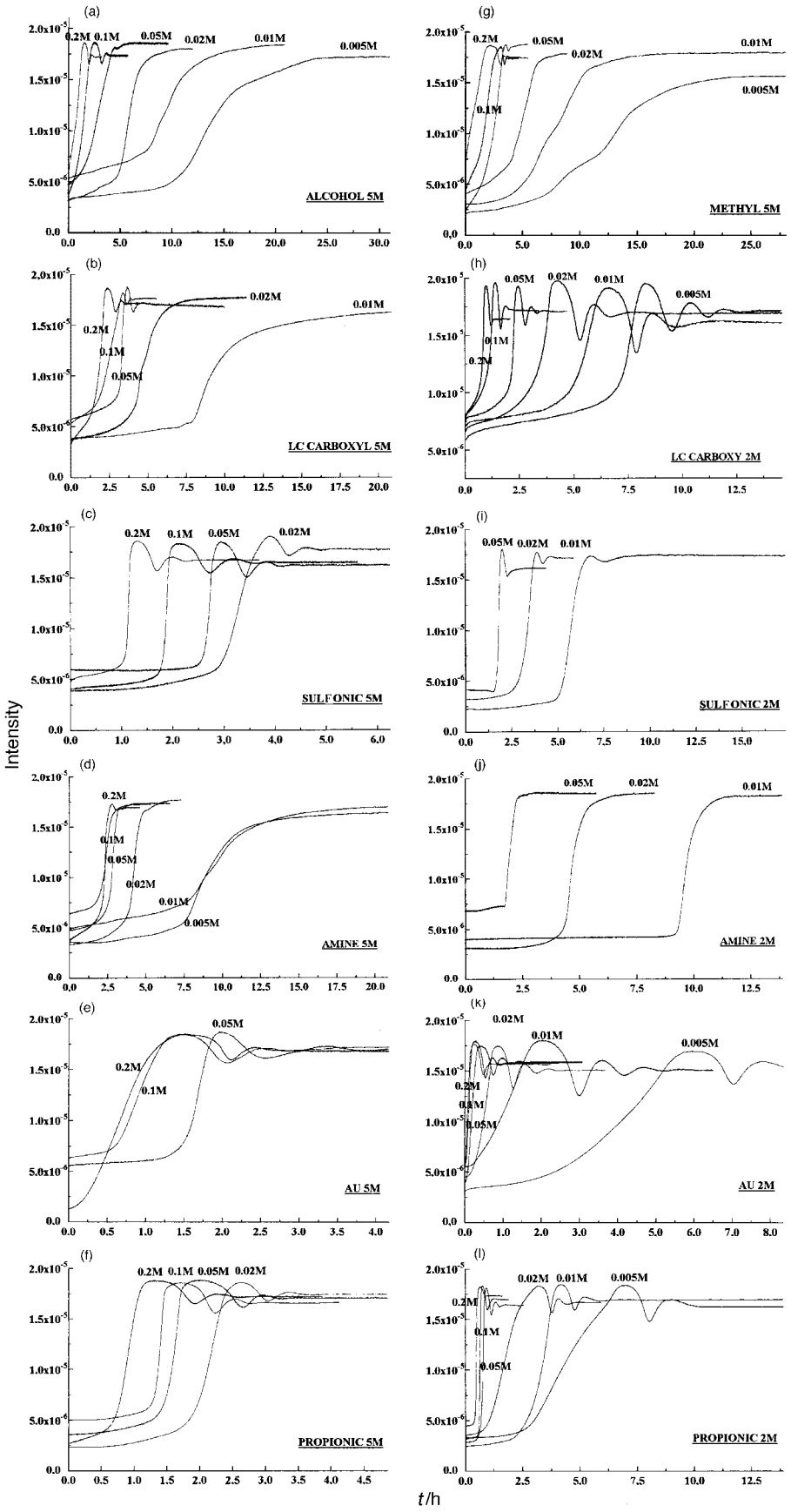

Fig. 1 Surface plasmon kinetic data for PbS deposition on the (a) alcohol, (b,h) long-chain carboxylic acid, (c,i) sulfonic acid, (d,j) amine (e,k) gold substrate, (f,l) propionic acid and (g) methyl SAMs from solutions prepared with the (a)–(g) 5 M NaOH solution and (h)–(l) 2 M NaOH solution.

the data shown are representative of 4–5 experiments. Curves in which the intensity attains a constant value without showing any oscillations correspond to the deposition of a thin film. Experiments in which reproducible data could not be obtained are not shown. In these cases little or no deposition occurred and any PbS growth was usually inhomogeneous over the substrate.

The results demonstrate that the 2 M deposition solution is more selective of substrate than the 5 M solution. The bare gold substrate, and the long-chain carboxylic and propionic terminated SAMs, all supported PbS deposition from the 2M solution over all TU concentrations, and all of these curves show oscillations, demonstrating formation of thicker films even at low TU concentration. The sulfonic-terminated thiol produced films over the range 0.1 to 0.01 M TU. The amine SAM showed limited deposition in the TU range 0.05 to 0.01 M, and even under these conditions produced thin films. The alcohol and methyl terminated thiols were very poor substrates, with the alcohol only allowing deposition from the 0.2 M TU solution (data not shown) and the methyl terminated thiol not supporting any growth. In contrast, the 5 M solution deposited films on all of the substrates used. Notably, the methyl and alcohol terminated SAMs, which were the only substrates not to allow film growth from the 2 M solution, supported growth over the entire concentration range of TU. The long chain carboxylic SAM showed deposition for all but the 0.005 M TU solution. The amine SAM, which only deposited from the 2 M solution for a limited range of TU concentrations, also supported PbS growth over the full range of TU concentrations. However, none of the kinetic curves for the low TU concentrations displayed oscillations, demonstrating that only thin films were deposited. This is consistent with the SEM data (see below). The gold, propionic and sulfonic SAMs which had been active for the 2 M solution preparations showed limited range, only depositing at the higher TU concentrations.

A measure of the influence of the surface functionality on the deposition of PbS was obtained by determining induction times from the kinetic curves. In nucleation theory the induction time is defined as the time elapsed between the creation of supersaturation and the detection of a new phase in solution. Necessarily, it is not a fundamental property of the system but depends upon the method used to locate the new phase. The induction time was taken as the intercept between the linear rise and the baseline of the kinetic curve, since this provides a representative characteristic of the kinetic curves, and simply provides a basis for comparing the influence of the different substrates.[60–63]

Data of induction time *versus* thiourea concentration are plotted in Fig. 2(a) and (b) for the 2 and 5 M solutions respectively. For the 2 M solution, the induction times increase in the order Au, propionic, long chain carboxylic, sulfonic and amine for the majority of the TU concentrations. The values of t_{ind} are also most insensitive to changes in TU concentration for the gold and propionic SAM substrates. The 5 M solution results are less clear cut, showing variation in the effectiveness of the SAMs over the range of TU concentrations. For the rapid depositions, the most effective substrates were the gold and the alcohol and propionic SAMs. At low TU concentrations, where many of the substrates were not active in supporting PbS deposition, the amine, methyl and alcohol terminated SAMs were most effective.

X-Ray diffraction

XRD was run in reflection of the PbS samples on Au/glass, yielding information on the orientation of the PbS crystals with respect to the gold substrate; no information is gained on the crystal orientation in the plane of the substrate. Table 1 displays the ratios of the diffraction peak intensities for the major {111}, {200} and {220} reflections. The values are presented, for ease of comparison, as relative to the lowest of the three intensities (set as 1). Direct comparison of the relative intensities of the {111} and {200} reflections is given, where necessary, in parentheses. The relative intensities anticipated for a powder sample of PbS are presented in Table 2. While some variation in the absolute values occurs between similar samples, the data presented are from the PbS films examined by SEM and are entirely representative. The data clearly show that, for samples that exhibit a preferred orientation, deposition from the 2 and 5 M solutions produces {100} and {111} orientations respectively, where these planes are parallel to the substrate. Polycrystalline samples that deviate strongly from complete randomness are said to be textured.[64] The strongest

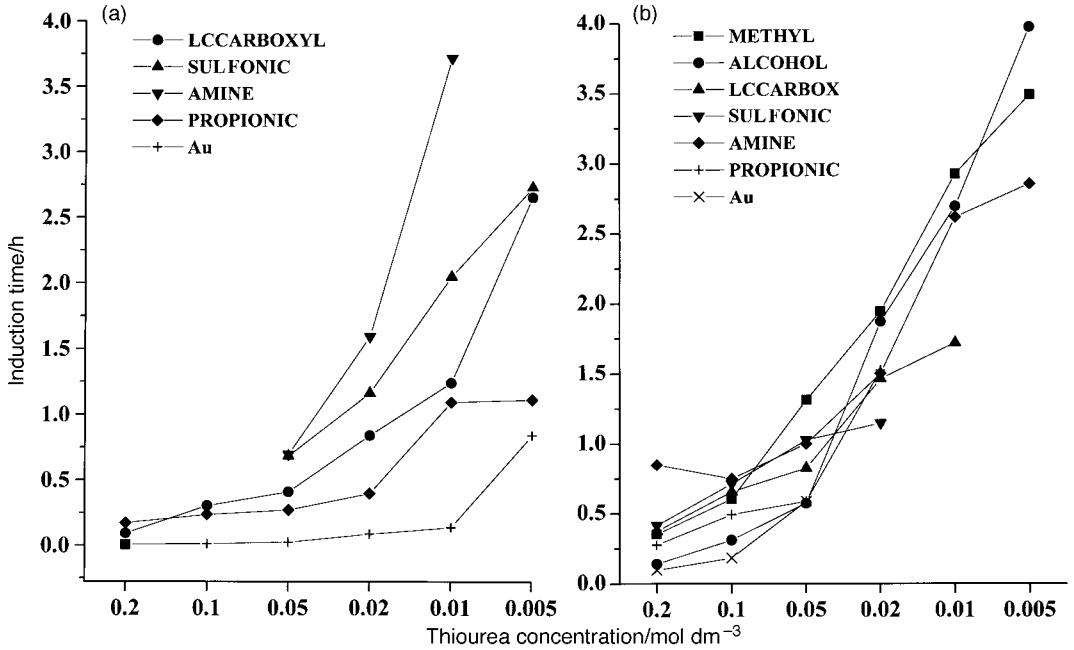

Fig. 2 Graphs of induction times for PbS deposition on the range of substrates for films prepared from the (a) 2 M NaOH solution and (b) 5 M NaOH solution.

Table 1 Summary of data of SEM and XRD analyses of PbS samples: crystal size, morphology and orientation information for PbS films formed on each substrate, for both the 2 and 5 M depositions. The XRD results are presented as relative intensities for the 111, 200, and 220 reflections. The relative intensities of the 111 and 200 reflections are additionally given in parentheses, when not previously presented

Thiourea conc./M	Crystal size/nm	Film structure	{111}	{200}	{220}
Alcohol					
2 M					
0.2	40–160	90% coverage. Intergrown, slightly indistinct morphologies. Blocky, rounded edges	3.39 (1)	4.38 (1.26)	2
0.1	190	30% coverage. Isolated crystals, spherical morphology			
0.05	—	No deposition			
0.02	—	No deposition			
0.01	—	No deposition			
0.005	—	No deposition			
5 M					
0.2	70–150	100% coverage. Distinct cubic morphologies. No pronounced orientation	3.60 (1.15)	3.13 (1)	1
0.1	70–280	100% coverage. Very distinct cubic crystals, mixed orientations	2.84 (1.12)	2.54 (1)	1
0.05	500	A few gaps in coverage. Very distinct cubic crystals. Mixed orientations	3.40 (1.35)	2.52 (1)	1
0.02	800	70% coverage. Well defined crystals, rounded edges			
0.01	920	70% coverage. Intergrown, floral morphologies			
0.005	580	70% coverage. Morphologically indistinct			
(b) Long chain carboxylic acid					
2 M					
0.2	56	100% coverage. Uniform particle size distribution. No distinct morphology	2.70 (1.1)	2.45 (1)	1
0.1	23–100	100% coverage. No marked morphology	3.11 (1.09)	2.85 (1)	1
0.05	45–160	100% coverage. Distinct cubic morphologies	3.42 (1.05)	3.24 (1)	1
0.02	52–260	Larger particle size distribution. Crystals are flatter and have irregular shapes	1.23 (1)	4.58 (3.27)	1
0.01	40–110	Morphologies not well defined, particles irregular. Some gaps in film	2.12 (1)	23.0 (10.9)	1
0.005	45–200	Morphologies not well defined. Particles textured. Larger particle size distribution (psd), some gaps in film	1.91 (1)	3.48 (1.82)	1
5 M					
0.2	60–240	100% coverage. Cubic crystals, oriented as in Fig. 4(g). Uniform psd.	2.84 (1.04)	2.73 (1)	1
0.1	50–220	100% coverage. Cubic with rounded edges, oriented as in Fig. 4(h),(i). Uniform psd	4.44 (2.07)	2.15 (1)	1
0.05	480	Some holes in film. Coverage mostly complete. Cubic crystals, oriented as in Fig. 4(h),(i)	3.91 (1.23)	3.18 (1)	1
0.02	690	Coverage virtually complete. Well defined angular morphologies	3.52 (1.19)	2.97 (1)	1
0.01	160–330	A few gaps in film coverage. Morphology less distinct, rounded edges, larger psd	3.41 (1.22)	2.80 (1)	1
0.005	380–440	A few gaps in film coverage. Large, blocky particles with rounded edges, stepped crystal faces. Uniform psd	3.00 (1.03)	2.91 (1)	1
(c) Sulfonic acid					
2 M					
0.2	—	—			
0.1	—	—			
0.05	280	Coverage almost complete. Rounded edges, uniform psd	2.23 (1)	10.16 (4.56)	1
0.02	190	80% coverage. Structure less clear. Some gaps, some adhesion larger particles	1	5.3	1.06
0.01	50–160	70% coverage. Irregular morphologies. Large psd	2.23 (1)	2.77 (1.24)	1
0.005	—	—			
5 M					
0.2	290	100% coverage. Morphology cubic with slightly rounded edges. No distinct orientation	4.82 (2.71)	1.78 (1)	1
0.1	240	100% coverage. Cubic crystals, uniform psd	5.18	1	2.27
0.05	420	100% coverage. Well-defined cubic morphologies. Crystals vertex oriented	15	1	2.27
0.02	340	100% coverage. Blocky crystals, rounded edges. No distinct orientation	3.39 (2.88)	1.18 (1)	1
0.01	—	—			
0.005	—	—			

Table 1 (*continued*)

Thiourea conc./M	Crystal size/nm	Film structure	{111}	{200}	{220}
(d) Amine					
2 M					
0.2	80	—			
0.1	110	—			
0.05	200	More uniform coverage, 50%. Cubic with rounded edges	3.00 (1.06)	2.84 (1)	1
0.02	300	Coverage 50%. Morphology cubic, better defined than 0.05 M. Crystals flat on substrate	2.89 (1.24)	2.34 (1)	1
0.01	320	Coverage 70%. Intergrown, rounded morphologies	3.38 (1.25)	2.7 (1)	1
0.005	—	—			
5 M					
0.2	290	80% coverage. Cubo-octahedral, facetted morphology	3.90 (1)	4.21 (1.08)	1
0.1	300	80% coverage. Cubo-octahedral, facetted morphology	4.0 (1)	4.0 (1)	1
0.05	310	Some gaps in film. Cubo-octahedral, facetted morphology. No clear orientation	4.44 (1)	5.24 (1.18)	1
0.02	420	Some gaps in coverage. Basic cubic morphologies, rounded edges	3.70 (1)	4.48 (1.21)	1
0.01	610	70% coverage. Morphology less distinct, spherical	2.71 (1)	3.32 (1.23)	1
0.005	760	80% coverage. Similar to 0.01 M, spherical	3.17 (1)	3.77 (1.19)	1
(e) Gold					
2 M					
0.2	50	Complete coverage, uniform psd. Spherical morphology	2.01 (1)	11.27 (5.44)	1
0.1	50–120	Complete coverage. Distinct morphologies with rounded edges	1	2.17	1.44
0.05	60–130	Complete coverage. Morphology clearer than 0.1 M, cubic with rounded edges	1.75 (1)	116 (66.3)	1
0.02	70–150	Full coverage, uniform psd. More blocky/cubic morphologies	1.02 (1)	56.8 (55.7)	1
0.01	40–200	Full coverage, large psd. Morphology less distinct	1.95 (1)	105.7 (54)	1
0.005	60–80	Complete coverage. Morphology indistinct. Some larger particles, later adherence?	1.18 (1)	25.5 (21.6)	1
5 M					
0.2	90–220	100% coverage. Angular crystals	3.50 (3.18)	1.10 (1)	1
0.1	140–280	100% coverage. Cubic crystals, very distinct morphologies	31.4 6.16	5.1 1	1
0.05	100–290	Complete coverage. Angular crystals, distinct morphologies	6.82	1	1.23
0.02	Small 50 Large 520	Coverage incomplete. Mixture of morphologies, smaller crystals + very large particles			
0.01	1000	Incomplete coverage. Intergrown platelets, florets, distributed over surface			
(f) Propionic acid					
2 M					
0.2	50–90	100% coverage, uniform psd. Approx. spherical crystals, some straight edges	4.7 (1.31)	3.6 (1)	1
0.1	50–150	100% coverage. Larger crystals, with rounded edges, fairly flat	1.90 (1)	2.40 (1.26)	1
0.05	60–160	100% coverage. Cubic crystals with rounded edges. Morphology more distinct, fairly flat	1.93 (1)	6.61 (3.42)	1
0.02	30–190	100% coverage. Irregular/cubic with rounded edges. Fairly flat	1	2.57	1.13
0.01	50–260	Full coverage. Irregular morphologies, cubic with kinky edges	1.52 (1)	13.5 (8.88)	1
0.005	180	100% coverage. Morphology indistinct, with textured faces (as Fig. 4(f))	2.88 (1)	9.6 (3.33)	1
5 M					
0.2	70–210	100% coverage. Distinct cubic morphologies. Appears quite oriented, many vertices	4.63 (3.22)	1.44 (1)	1
0.1	90–270	100% coverage. Distinct cubic morphologies. Appears quite oriented, many verteces	8.20	1	2.84
0.05	120–400	Complete coverage. Distinct cubic morphologies. Appears quite oriented, many vertices	23.4	1	2.98

Table 1 (*continued*)

Thiourea conc./M	Crystal size/nm	Film structure	{111}	{200}	{220}
0.02	80–420	Coverage complete. Somewhat less distinct morphologies with more rounded edges. Appears oriented	16.1	1	4.90
0.01	—	—			
0.005	—	—			
(g) Long chain hydrocarbon					
No deposition from 2 M solution					
5 M					
0.2	120–330	100% coverage. Very distinct cubic morphologies, as in Fig. 4(h),(i)	4.22 (1.14)	3.70 (1)	1
0.1	100–290	100% coverage. Distinct cubic morphologies, as in Fig. 4(h),(i)	2.22 (1)	2.58 (1.16)	1
0.05	140–330	100% coverage. Distinct cubic morphologies, as in Fig. 4(h),(i)	4.27 (1)	4.74 (1.11)	1
0.02	370–730	70% coverage. Spherical particles	2.67 (1)	3.46 (1.30)	1
0.01	Plates 450	70% coverage. Platy particles, forming floret-like clusters [as in Fig. 4(k)]	3.82 1.15	3.31 1	1
0.005	Plates 540	70% coverage. Platy particles, forming floret-like clusters [as in Fig. 4(k)]	3.09 1.02	3.03 1	1

Table 2 Powder diffraction data for PbS (Powder card 5–592). Higher reflections, all of low intensity are not shown

d/Å	2θ/°	I/I_1	hkl
3.429	30.242	84	111
2.969	35.068	100	200
2.099	50.447	57	220
1.790	59.962	35	311
1.714	62.916	16	222
1.484	74.135	10	400
1.362	82.104	10	331
1.327	84.763	17	420
1.212	95.127	10	422

orientation effects are seen in the mid-range TU concentrations, usually 0.05 and 0.02 M TU. The most oriented samples are those grown on the gold and the propionic acid SAMs. In the case of the gold substrate the 2M samples at TU concentrations of 0.05, 0.02 and 0.01 M are almost exclusively {100} oriented, while the 5 M NaOH and 0.1, 0.05 and 0.02 M TU samples are strongly {111} oriented. The propionic acid SAMs show marked {111} orientational control for the 5M solution at 0.05 and 0.02 M TU. The sulfonic acid and long-chain carboxylic SAMs show some influence. The sulfonic SAM at 0.05 M TU was clearly {111} oriented in the 5 M case and {100} oriented in the 2 M solution, while the long-chain carboxylic SAM shows {100} orientation for the 2 M solution at 0.02 and 0.01 M TU. No pronounced orientational effects are seen for the alcohol, methyl or amine samples.

Examples of the XRD spectra are shown in Fig. 3. A pronounced {100} orientation is shown in Fig. 3(a) for PbS deposited on the gold substrate, from the 2 M NaOH stock solution and 0.05 M TU. Fig. 3(b) shows {111} oriented PbS crystals deposited on the propionic substrate, from the 5 M NaOH stock solution and 0.05 M TU. Examination of the gold substrates prior and subsequent to heat treatment showed almost exclusive {111} orientation.

SEM Studies

The morphology of the PbS films at the termination of growth was investigated using SEM. Descriptions of the films in terms of the size and morphology of the PbS crystals for samples prepared from the 2 and 5 M solutions over the range of TU concentrations are given in Table 1. As an illustrated example, images of the film structures for PbS deposited on the gold

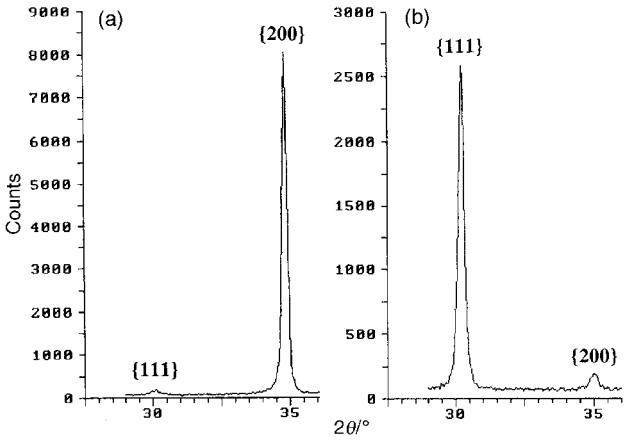

Fig. 3 XRD spectra of (a) PbS on gold substrate, from the 2 M NaOH stock solution and 0.05 M TU and showing strong {200} orientation; (b) PbS on the propionic acid substrate, from the 5 M NaOH stock solution and 0.05M TU, and showing a pronounced {111} orientation.

substrate are shown in Fig. 4, such that the structural variations resulting from changes in the TU concentration and the solution pH can readily be compared.

Distinct morphological differences occur between the PbS films grown on Au under different conditions. The 2 M samples comprise crystals of basic cubic morphologies, oriented with a face approximately parallel to the substrate, as is consistent with the {100} orientation measured by XRD. The crystals are best oriented in samples 4(c) and 4(d), corresponding to the mid-range TU concentrations 0.05 and 0.02 M. At slower deposition rates the crystal morphologies are indistinct and there is a larger particle size distribution. However, on the basis of the XRD results these samples remain well oriented, more so than the rapidly grown samples of TU concentrations 0.2 and 0.1 M shown in 4(a) and 4(b). The 5M samples [Fig. 4(g) and 4(h)] show larger crystals with very distinct cubic morphologies. A larger particle size distribution is apparent compared with the 2 M samples. Clearly, the orientation of the crystals is quite different from the 2 M case, as anticipated from the XRD results which reveal a marked {111} orientation. The crystals shown in Fig. 4(g)–(i) are cubes, oriented such that a vertex is uppermost (*i.e.* viewed down the $<111>$ axis). Samples 4(j) and 4(h) are poor quality films as also demonstrated by the irreproducibility of the kinetic

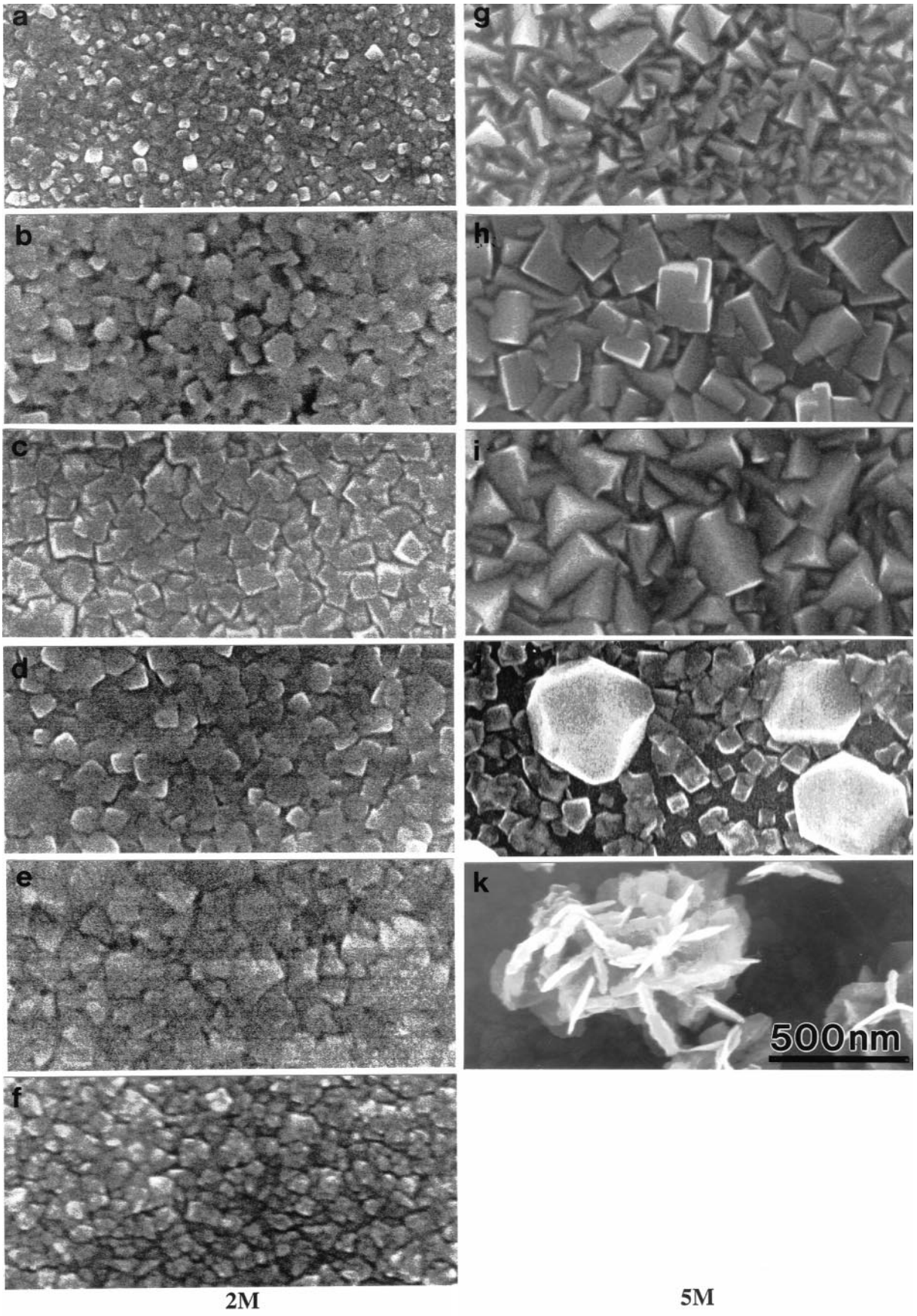

Fig. 4 SEM images for PbS deposited on the gold substrates from the 2 M NaOH solution and thiourea concentrations (a) 0.2, (b) 0.1, (c) 0.05, (d) 0.02, (e) 0.01, (f) 0.005 M, and from the 5 M NaOH solution and thiourea concentrations (g) 0.2, (h) 0.1, (i) 0.05, (j) 0.02 and (k) 0.01 M.

measurements under these solution conditions. Sample 4(j) shows incomplete film growth and the presence of some very large particles, possibly adsorbed from solution at later stages of film growth. Sample 4(k) comprises large clusters of platy crystals, intergrown to give floret morphologies. An increase in crystal size occurs from 4(g) to 4(h), although percentagewise to a lesser extent than the 2 M samples.

As described in Table 1, the trends occurring over the series of samples grown on the gold substrate are consistent with observations made on PbS films deposited on the other substrates. The 2 M samples show considerably smaller crystal sizes than their 5M counterparts, and smaller particle size distributions. For both sets of samples the crystal size tends to increase with a decrease in the TU concentration. In all cases the morphology tends towards cubic, as reflects the FCC (face centred cubic) crystal system of PbS. The morphology is clearer and more angular in the 5 M case, possibly due to the larger size of the crystals, while the crystals grown from the 2 M solution tend to a more rounded form. Importantly, crystals in the 5 M samples exhibit a {111} orientation, which results in the cubes placed vertex-uppermost while the 2 M samples have a preferred {100} orientation, which appears as the cube face parallel to the substrate. For both the 2 and 5 M solutions, the morphologically best-defined crystals correlate with mid-range TU concentrations, typically 0.05 and 0.02 M. This is also coincident with the best-oriented samples, as measured by XRD. Samples in which the coverage of the substrate by PbS crystals is incomplete are typically characterised by a larger particle size. This suggests that, under these solution conditions, film formation is nucleation limited; subsequent to nucleation, crystal growth is controlled by the available area and reactant concentrations.

The SAM selected as the substrate clearly influences the structure of the deposited film, as does the pH of deposition. Deposition from the 2 M solutions is more dependent on the substrate than the 5 M solution depositions. The long-chain carboxylic acid and propionic SAMs and the bare gold substrate all support growth of complete films from the 2 M solution over the entire range of TU concentrations. The amine- and sulfonate-terminated SAMs allow some growth, but film coverage is generally incomplete. For both of these substrates the coverage is superior for fairly low TU concentrations; the 0.2, 0.1 and 0.005 M solutions produce very thin films and exhibit poorly reproducible growth kinetics. No, or extremely limited, deposition occurs on the alcohol and the hydrocarbon monolayers. The 5 M solutions are less selective of substrate, all supporting deposition over at least four TU concentrations. Deposition is superior for higher TU concentrations, low concentrations typically producing incomplete film coverage and larger particle sizes. Even substrates that do not exhibit film growth from the 2 M solution (notably the hydrocarbon and alcohol thiols) yield high quality, complete coverage films from the 5 M solution. However orientation effects are less pronounced for the 5 M than for the 2 M solution.

TEM Studies

The TEM studies provide some information on the growth mechanism of the film. The films were monitored over time to show their structural evolution. The very thin films showed areas of extremely small particles on the substrates. Growth resulted in the formation of two distinct domains of crystals, clusters of small crystallites and areas of well defined particles. Fig. 5(a) and (b) show the former type of crystals, deposited on the long-chain carboxyl substrate, from the 2 M solution and 0.2 M TU. The particle size is very small at around 2 nm in Fig. 5(a), while clusters of 5 nm particles are viewed in Fig. 5(b). The particles are apparently embedded in a diffuse background. Film growth results in an increase in particle size to approximately 20 nm, and in the growth or adsorption of further clusters of particles on the primary layer [Fig. 5(c)]. SEM examination of fully grown films revealed a particle size of 50 nm. The alternative mechanism of crystal growth is shown in Fig. 5(d) and (e) which corresponds to some areas of deposition on the long-chain carboxyl substrate from the 5 M solution and 0.2 M TU. The crystals in Fig. 5(d) are distributed over the substrate and are in the order of 20 nm in diameter. Fig. 5(e) shows an increase in the number of crystals to produce a close-packed array of particles 40–50 nm in size. The SEM images of this film showed crystals of diameters 60–240 nm. Study of the other systems revealed similar results. In particular, the images of the PbS deposition on the alcohol SAM from the 5 M, 0.2 M TU solution were very clear, showing the presence of 50–70 nm clusters of smaller, but well defined 10–20 nm crystallites [Fig. 5(f)]. The SEM studies showed particles of diameters 70–150 nm. The images suggested that the two types of crystal growth were quite distinct. The clusters of very small particles formed uniformly over an entire area, in a diffuse background. Increase in the film thickness resulted in growth of these particles, and in conversion of the diffuse material into crystals [Fig. 5(f) shows this clearly]. The alternative mechanism of film growth showed well defined crystals, which were non-aggregated and produced in the absence of the background amorphous matrix. These crystals increased in density and size to produce a close-packed array over the substrate.

Diffraction patterns were also measured for the samples. All indicated that PbS and Au were the only crystalline phases present; no crystalline lead hydroxide phases were detected. Diffraction patterns were taken in selected area mode, either within a single gold crystal or over a larger area of the substrate to yield a powder-type pattern. Diffraction patterns were taken of all samples, but the samples in which XRD analyses had suggested that the PbS crystals were oriented will be emphasised: gold substrate, 2 and 5 M NaOH, 0.05M TU; gold substrate, 2 M NaOH, 0.2 M TU; propionic acid SAM, 2 and 5 M NaOH, 0.05 M TU. Results were compared with samples in which no orientational effects had been observed, such as the long chain carboxyl and alcohol SAMs for deposition from 5 M NaOH solution, 0.2 M TU. In all cases, when the gold crystal was of large enough diameter to permit selected-area diffraction within the crystal, the resultant single crystal patterns were all indexed as $<111>$ zone [Fig. 6(a)]. The patterns showed additional reflections, beyond those anticipated for a $<111>$ zone: {220}, {422}, {440}, *etc.* These are due to diffraction from the second Laue zone. Extension of the diffraction rods due to the small thickness of the sample, and warping of the Ewald sphere due to bending of the crystal in the beam can result in the additional reflections seen. Powder patterns showed all anticipated gold reflections, but with enhanced {220} reflections, indicating preferential {111} orientation. In all cases a powder diffraction pattern characteristic of PbS was superimposed on the gold pattern [Fig. 6(b)]. No epitaxial matching between the PbS crystals and the supporting gold substrate was observed for either the gold single crystal or powder pattern configuration. Surprisingly, there was also no evidence of preferred orientation of the PbS crystals in any of the samples. On the basis of the XRD results it had been expected that some of the samples would have shown preferred {111} or {100} orientation of PbS crystals at early stages of the film growth. In the majority of patterns all of the reflections at d spacings larger than 1.790 Å, PbS {311} were observed; the low intensities of higher order reflections precluded their observation. The gold {200} ($d=2.039$ Å) and PbS {220} ($d=2.099$ Å) reflections are too close to enable them to be distinguished. In the case of some patterns measured of the Au 2 M, 0.2 M TU system the PbS {111} reflection was absent.

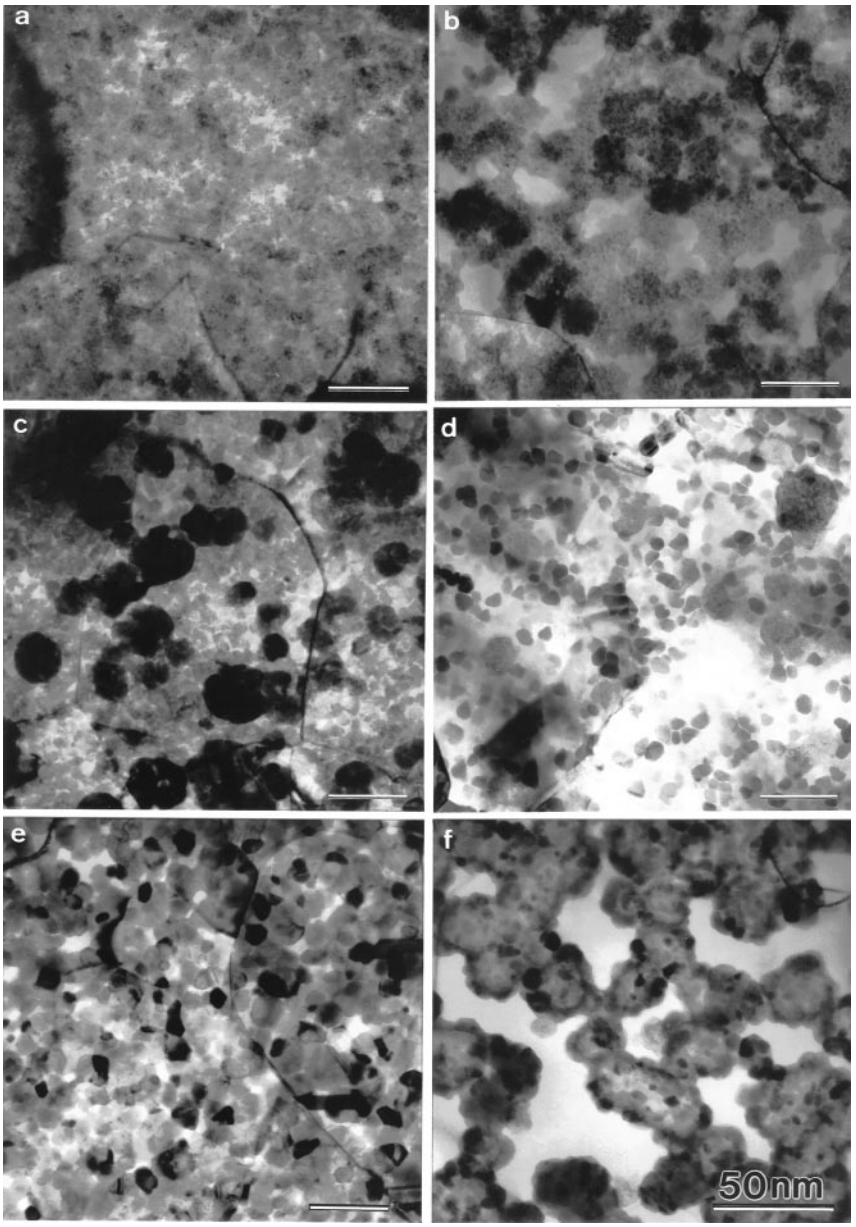

Fig. 5 TEM images for the early stages of deposition of PbS on the long-chain carboxyl substrate from (a)–(c) the 2 M NaOH stock solution and 0.2 M thiourea, (d)–(e) the 5 M NaOH stock solution with 0.2 M thiourea. Fig.(f) shows an area of deposition of PbS on the alcohol substrate from the 5 M NaOH stock solution, with 0.2 M TU. All scale bars = 50 nm. Fig.(a)–(e) are at the same magnification while (f) is at a higher magnification.

Discussion

The experiments demonstrated that the substrate and the SAM terminal group was effective in influencing the nucleation and growth rates of the PbS films, the size of deposited crystals and the final orientation of crystals in the films. Other investigations into the chemical deposition of PbS have shown that this method can be used to produce epitaxial growth of PbS on single crystal substrates of {111} Ge and {111} Si.[65–68] Powder crystalline films were produced on glass surfaces.[67]

Chemical deposition is proposed to proceed either by an ion-by-ion mechanism, in which the crystals nucleate and grow on the substrate, or *via* a cluster mechanism in which nuclei of the metal sulfide or metal hydroxide form in solution and then adsorb onto the surface when the film thickness can increase by particle growth or through further adsorption of particles. The mechanism operating depends upon the solution conditions and defines the quality of the final film produced. The chemical deposition of PbSe has been studied in detail, and was shown to be dependent on the relative concentrations of the Pb^{2+} ion and the complexing agent used.[11,12] At low concentrations of the complexing agent (LC) a hydroxide-mediated mechanism occurred. Some lead hydroxide formed in the solution, and these particles adsorbed on to the surface. Further reaction with the Se^{2-} species results in the production of small PbSe particles. This mechanism can still occur when the hydroxide colloids are too small to be visible to the naked eye. LC films often showed an amorphous matrix of PbSe surrounding the crystals, and typically also contain domains of larger crystals, which increase in size as the film thickness increases. High concentrations of the complexing agent (HC) precluded formation of the hydroxide, and an ion-by-ion growth mechanism was operative. Larger crystals were produced. Deposition of PbSe over a range of concentrations $KOH:Pb^{2+}$ was investigated, with 5–10 : 1 clearly corresponding to the LC regime and 36–72 : 1 to the HC regime. Dissolution of the Pb–OH colloidal phase occurred over time so extremes in the concentration range were examined. The LC films comprised small crystallites of sizes 3–7 nm, which were homogeneously distributed over the surface. The crystals in the corresponding HC films were well defined square crystals, 300–500 nm in cross-section. It was also shown that

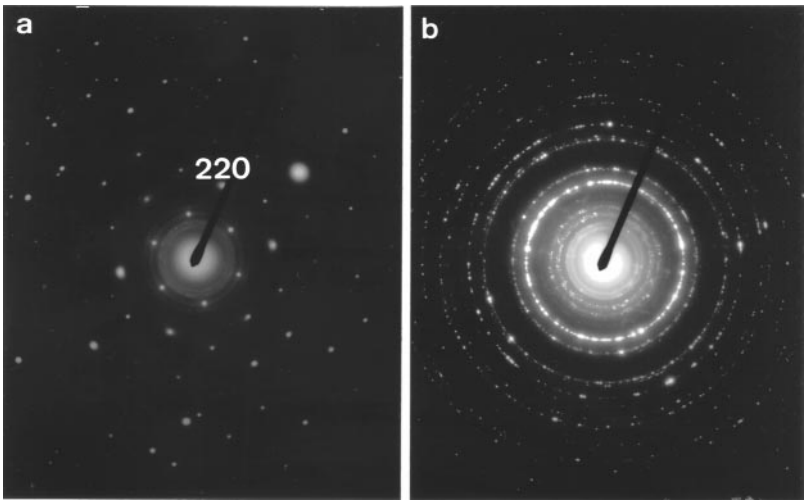

Fig. 6 Diffraction patterns of PbS deposited on the gold substrate from (a) the 2 M NaOH stock solution and 0.2 M TU, and (b) the 5 M NaOH stock solution and 0.2 M TU; (a) is taken of a selected area within a single gold crystal where the discrete set of spots derive from the crystal and the rings are from PbS crystals, while (b) encompasses a larger area and many gold crystallites, thus showing superimposed gold and PbS powder patterns.

the solution pH may play an important role in determining the film structure.[11] Incubation of a LC PbSe film in strong alkaline solution resulted in an increase in crystal size, indicating that a dissolution–reprecipitation process was occurring.

Our present experimental conditions correspond to $KOH:Pb^{2+}$ of 10 and 25:1 for the 2 and 5 M deposition solutions respectively. According to the analysis of Gorer *et al.*[11,12] the 2 M solution would be clearly in the LC regime, while both the LC and HC mechanisms may be operative in the 5 M solution (although it should be noted that we are here depositing PbS which has a higher solubility product than PbSe). The data described here are fairly consistent with this analysis. No marked difference was observed at the thin film stage between the 2 and 5 M depositions. The TEM data generally showed an initial deposition of small particles of 5–10 nm from both the 2 and 5 M solutions, often in an amorphous background. Growth of the films occurred by an increase in the number of particles and of the particle size and definition. Some areas showed densely packed crystals of very well defined morphologies. Once a homogeneous covering of crystallites had been produced there was also some evidence of adsorption of larger particles, probably formed as clusters of smaller crystallites. It may be reasonably suggested that a mixture of mechanisms is active in the current experiments. The small particles may derive from absorption of a lead hydroxide species, followed by conversion into PbS, and further growth on the substrate. The larger particles with very distinct morphologies may form by an ion-by-ion mechanism. As stated earlier, under the alkaline conditions of the experiments, some structural changes may occur post-deposition due to dissolution/reprecipitation, which will be more pronounced in the 5 M solution. This mechanism may also contribute to the larger average crystal size and size distribution observed in the 5 M solution.

This is also consistent with both the SEM and kinetics results. The hydroxide mechanism will be more active for deposition from the 2 than from the 5 M solution, since a higher hydroxide ion concentration favours the formation of the soluble hydroxide complex $HPbO_2^-$.[12] Thus, for the 2 M solution, the primary mechanism may be *via* adsorption and reaction of insoluble lead hydroxide particles, producing a more uniform population of smaller PbS crystals. On increasing the concentration of NaOH in the 5 M solution the stability of the $HPbO_2^-$ complex is increased and the cluster mechanism suppressed. Both the cluster and ion-by-ion mechanisms may act, resulting in a larger particle size distribution and in larger particle sizes. The crystal size increase from the 2 to 5 M solution may also be directly influenced by the increasing pH. Incubation in strong alkaline solutions of PbSe films that had been deposited in the LC region resulted in an increase in the crystallite size,[11] suggesting that the crystals were undergoing a dissolution and reprecipitation process. The hydroxide mechanism would also be anticipated to be more substrate-specific than the ion-by-ion. While all of the substrates will be charged under the experimental conditions, and thus be active for the ion-by-ion mechanism, colloidal hydroxide particles can either adsorb on to the substrate or grow and react in the bulk solution to form PbS. The hydroxide mechanism would thus be imagined to be more surface specific. The 5M depositions were also considerably slower than those from the 2M solutions. The ion-by-ion mechanism would be anticipated to be slower than the cluster mechanism since the hydroxide and PbS surfaces can act catalytically to increase the rate of thiourea decomposition.[65]

The gold and propionic acid SAMs showed the most pronounced influence over crystallisation, exhibiting the lowest induction times, supporting deposition over a wide range of experimental conditions and influencing the formation of highly oriented films. The sulfonic and the long-chain carboxyl SAMs were also fairly effective in influencing the rate and orientation of the growing films. The alcohol, methyl and amine surfaces did not provide good growth substrates. Thus, PbS crystals deposit most readily on the SAMs bearing terminal groups with the highest dissociation constants. That the Au is also very effective may be in part because the surface is very ordered in comparison with the SAMs. The Au is also a good conductor which will limit excess charge build up on the surface during the adsorption of ions from the reaction solution,[44] thus facilitating further adsorption. Both the propionic and sulfonic acid SAMs are short-chain thiols and thus form poorly ordered monolayers. The longer-chain SAMs are considerably more ordered, due to interactions between the hydrocarbon chains, but studies have shown that the headgroups may still be disordered.[31] The issue of preferred orientation in the PbS films is hard to explain. Since only some of the substrates influenced a unique directionality in the fully grown films, it would be imagined that this control by the surface must be active at the nucleation stage. However, the electron diffraction studies provided no evidence for this, either in selected area patterns measured within a single large gold crystal or from over a larger area and many gold crystals. A

range of samples were examined in detail, particularly those that had shown marked orientation effects in the XRD measurements. This topic will be studied in detail in further work.

A number of other studies have been made on the influence of SAMs on crystal growth, particularly of calcium carbonate, and some have also demonstrated an effect on the crystal orientation. Calcium carbonate was grown on a range of functionalised organosilane monolayers, and the expressed terminal group was demonstrated to influence the final orientation of the crystals.[46] Calcite grown on amino-modified surfaces was of the standard rhombohedral morphology and crystals lay on {104} faces. Surfaces of silicon oxide, carboxylate, iminodiacetate and phosphoramidate directed a near $<001>$ orientation of the crystals. The population density of crystals was also affected by the monolayer functionality with the highest density occurring for the carboxylate and iminodiacetate monolayers.

Functionalised thiol monolayers on gold have also been used as substrates on which to precipitate calcium carbonate.[44,47] In the study by Wurm *et al.*[47] amorphous calcium carbonate was produced on $C_{11}H$ and $C_{11}OH$ SAMs, while oriented calcite rhombs were observed on $C_{11}OOH$ surfaces and spherulitic vaterite crystals on C_9SH SAMs. No diffraction studies were carried out on these systems. However, the data indicated that the SAM was active in influencing the phase, and possibly the orientation of growing crystals. Küther *et al.*[44] carried out a detailed study on the influence of the SAM headgroup and chain length on the phase and morphology of calcium carbonate precipitated. Long and short chain thiols with COONa, SO_3Na, CH_3, OH, PO_3H and SH terminal groups were studied. As anticipated, the nucleation density was greatest on the polar surfaces. Crystals deposited on the $C_{11}OOH$ and $C_{16}OOH$ monolayers were predominantly calcite and vaterite respectively. Similarly, the shorter chain $C_{11}H$ thiol principally supported calcite deposition, while almost equal quantities of calcite and vaterite grew on the $C_{16}H$ SAMs. The crystals deposited on the $C_{10}SO_3H$ and C_3SO_3H monolayers were primarily calcite, and vaterite on the $C_{12}SH$ and $C_{16}SH$ monolayers. In general, the crystals were more oriented on the monolayers of short-chain as compared with the long-chain thiols. The range of sometimes conflicting results of calcium carbonate deposition on SAMs by the different authors also serves to suggest that precise experimental details such as the roughness and source of the substrate, the method of producing the gold film, and the conditions of the crystallisation strongly affect crystal nucleation and growth.

Organophosphonate mono- and multi-layers have also been used to prepare oriented arrays of zinco-phosphate zeolite crystals.[42] Immersion of the trilayer substrates in the zeolite solution resulted in the growth of crystals showing a 90% preferential {111} orientation. The orientation may have been defined by nucleation of crystals off the {111} face, or *via* adsorption of crystallites formed in the solution and continued growth on the substrate. Notably, the orientation effect was not observed for the corresponding monolayer system, suggesting that a fairly well ordered, homogeneous surface was required for favourable electrostatic interactions with the growing crystals. Iron oxyhydroxide (as α-FeOOH, goethite) was precipitated on sulfonic acid terminated alkylsilane monolayers[39,45] and the crystals were shown to be columnar in morphology and nucleated off a {010} plane.[45] Identical orientational effects were observed for sulfonated polystyrene surfaces, demonstrating that an ordered organic lattice is not required to induce orientation of an inorganic phase in the direction normal to the surface.

The relationship between surface-directed crystallisation and factors such as ion binding, surface charge density and interfacial ion concentrations has been quantitatively estimated by considering the electrostatic contributions of electrostatic parameters and ion distributions to nucleation at an interface.[69] Crystals nucleating on a surface form within a physically and chemically anisotropic double-layer environment, which is necessarily quite distinct from the bulk solution conditions. Calculations suggested that it is the cation to anion ratio at negatively charged surfaces, and not simply the cation concentration which is more traditionally considered, which is important in defining the nucleation process. Inter-ion repulsions at the surface lead to overall ion concentrations, which depart markedly from the lattice ion stoichiometry and can affect such factors as nucleation and growth rates, crystal solubilities and crystal phase. Additionally, the lower effective pH near negatively charged surfaces can also alter crystal supersaturation. The anion speciation at a charged surface was also suggested to influence oriented nucleation. Depending on the solution conditions, the chemical species adjacent to surfaces may be complex, especially at higher pH values. Some of these molecules exhibit a permanent dipole and thus may orient in the electric field at the surface. This mechanism may result in orientation of the nucleating crystals.

In our present experiments we might imagine that factors such as those proposed above may be responsible for producing orientational effects with some of the substrates. Indeed, X-ray reflectivity studies of 16-sulfanylhexadecanoic acid on gold single crystals in the presence of a range of counter ions including Cd^{2+}, Pb^{2+} and Ca^{2+} demonstrated that specific chemical interactions between the counter ion and the carboxylic group were more important than pure electrostatic interactions in forming dense counter ion overlayers.[70] It can be clearly stated that no form of geometrical match is required at the substrate/crystal interface, since the short chain propionic acid and sulfonic acids are poorly ordered monolayers and yet induce the formation of highly oriented PbS films. In these films the orientation of the crystals is defined normal to, but not in the plane of, the substrate. It is also notable that the PbS films deposited on the propionic SAMs were more ordered than those on the long-chain carboxyl substrates, despite identical terminal groups.

The control over crystal growth by SAMs can be compared with the action of other organic thin films. Of particular note, Langmuir monolayers at the air/water interface have been successfully used to direct oriented crystal growth. An epitaxial match between the organised monolayer and developing crystals has been achieved in a number of systems including aliphatic alcohols/ ice crystals[71,72] and arachidic acid/PbS and CdS.[73] The nucleating face and crystal phase of $CaCO_3$ crystals was defined by monolayers bearing carboxylic acid, amine and sulfate headgroups.[74] Langmuir monolayers thus offer a significantly greater degree of control than SAMs bearing corresponding headgroups. The principal difference between these systems is the order of the organic layer. While the air/water interface is ideally flat and the monolayer well crystalline, SAMs are formed on microscopically much rougher substrates and the terminal groups are often highly disordered. While SAMs can direct the nucleating face, they are apparently too disordered to achieve any direct match between the nucleating crystal face and molecular organisation of the SAM. Thus, a number of factors, including possibly the orientation of the exposed endgroups, seem to be important in influencing inorganic crystal growth on SAMs.

Conclusions

The research described demonstrates that self-assembled monolayers are active in controlling the rate of deposition, the size and orientation of chemically deposited PbS films. The orientation effect was very pronounced under certain growth conditions and was dependent on the substrate itself and on the NaOH concentration in the deposition solution.

The mechanism of growth control is not well understood, but will form the basis of further investigations.

Acknowledgements

F. C. Meldrum would like to thank the Alexander von Humboldt for funding a visiting fellowship.

References

1 S. Manne and L.A. Aksay, *Curr. Op. Sol. State. Mater. Sci.*, 1997, **2**, 358.
2 *ACS Symp. Ser.*, 1992, **499**.
3 *ACS Symp. Ser.*, 1997, **679**.
4 J. M. Phillips, *MRS Bull.*, 1995, 35.
5 F. F. Lange, *Science*, 1996, **273**, 903.
6 D. K. Russell, *Chem. Vap. Dep.*, 1996, **2,** 223.
7 M. Noh, C. D. Johnson, M. D. Hornbostel, J. Thiel and D. C. Johnson, *Chem. Mater.*, 1996, **8**, 1625.
8 A. C. Jones, *Adv. Mater.*, 1993, **5**, 81.
9 D. Lincot, B. Mokili, M. Froment, R. Cortes, M. C. Bernard, C. Witz and J. Lafait, *J. Phys. Chem. B*, 1997, **101**, 2174.
10 D. Lincot and R. Ortega-Borges, *J. Electrochem. Soc.*, 1992, **139**, 1880.
11 S. Gorer, A. Albu-Yaron and G. Hodes, *J. Phys. Chem.*, 1995, **99**, 16442.
12 S. Gorer, A. Albu-Yaron and G. Hodes, *Chem. Mater.*, 1995, **7**, 1243.
13 P. C. Rieke and S. B. Bentjen, *Chem. Mater.*, 1993, **5**, 43.
14 Y. Golan, B. Alperson, J. L. Hutchinson, G. Hodes and I. Rubinstein, *Adv. Mater.*, 1997, **9**, 236.
15 Y. Mastai and G. Hodes, *J. Phys. Chem. B*, 1997, **101**, 2685.
16 B. W. Gregory, D. W. Suggs and J. L. Stickney, *J. Electrochem Soc.*, 1991, **138**, 1279.
17 S. M. George, A. W. Ott and J. W. Klaus, *J. Phys. Chem.*, 1996, **100**, 13121.
18 T. Kanniainen, S. Lindroos, J. Ihanus and M. Leskela, *J. Mater. Chem.*, 1996, **6**, 161.
19 V. P. Tolstoi, *Russ. Chem. Rev.*, 1993, **62**, 237.
20 G. Decher, *Science*, 1997, **277**, 1232.
21 J. H. Fendler, *Chem. Mater.*, 1996, **8**, 1616.
22 J. Schmitt, G. Decher, W. J. Dressick, S. L. Brandow, R. E. Geer, R. Shashidhar and J. M. Calvert, *Adv. Mater.*, 1997, **9**, 61.
23 V. L. Colvin, A. N. Goldstein and P. Alivisatos, *J. Am. Chem. Soc.*, 1992, **114**, 5221.
24 M. D. Musick, C. D. Keating, M. H. Keefe and M. Natan, *J. Chem. Mater.*, 1997, **9**, 1499.
25 H. Fan and G. P. Lopez, *Langmuir*, 1997, **13**, 119.
26 F. C. Meldrum and J. H. Fendler, in *Biomimetic Materials Chemistry,* ed. S. Mann, VCH, New York, 1997.
27 B. O. Dabbousi, C. B. Murray, M. F. Rubner and M. G. Bawendi, *Chem. Mater.*, 1994, **6**, 216.
28 L. Motte, F. Billoudet, E. Laeze, J. Douin and M. P. Pileni, *J. Phys. Chem. B*, 1997, **101**, 138.
29 M. Giersig and P. Mulvaney, *Langmuir*, 1993, **9**, 3408.
30 E. Delamarche, B. Michel, H. A. Biebuyck and C. Gerber, *Adv. Mater.*, 1996, **8**, 719.
31 A. Ulman, *An Introduction to Ultrathin Organic Films*, Academic Press New York, 1991.
32 N. L. Jeon, W. Lin, M. K. Erhardt, G. S. Girolami and R. G. Nuzzo, *Langmuir*, 1997, **13**, 3833.
33 P. C. Hidber, P. F. Nealey, W. Helbig and G. M. Whitesides, *Langmuir*, 1996, **12**, 5209.
34 A. Kumar, H. A. Biebuyck and G. M. Whitesides, *Langmuir*, 1994,**10**, 1498.
35 F. C. Meldrum, J. Flath and W. Knoll, *Langmuir*, 1997, **13**, 2033.
36 E. L. Smith, C. A. Alves, J. W. Anderegg and M. D. Porter, *Langmuir*,1992, **8**, 2702.
37 H. Shin, R. J. Collins, M. R. DeGuire, A. H. Heuer and C. N. Sukenik, *J. Mater. Res.*,1995, **10**, 692.
38 H. Shin, R. J. Collins, M. R. DeGuire, A. H. Heuer and C. N. Sukenik, *J. Mater. Res.*, 1995, **10**, 699.
39 B. C. Bunker, P. C. Rieke, B. J. Tarasevich, A. A. Campbell, G. E. Fryxell, G. L. Graff, L. Song, J. Liu, J. W. Virden and G. L. McVay, *Science*, 1994, **264**, 48.
40 D. J. Dunaway and McCarley, *Langmuir*, 1994, **10**, 3598.
41 S. E. Gilbert, O. Cavalleri and K. Kern, *J. Phys. Chem.*, 1996, **100**, 12123.
42 S. Feng and T. Bein, *Nature* (*London*), 1994, **68**, 834.
43 W. J. Dressick, C. S. Dulcey, J. H. Georger and J. M. Calvert, *Chem. Mater.*, 1993, **5**, 148.
44 J. Küther, R. Seshadri, W. Knoll and W. Tremel, *J. Mater. Chem.*, 1998, **8**, 641.
45 B. J. Tarasevich, P. C. Rieke and J. Liu, *Chem. Mater.*, 1996, **8**, 292.
46 D. D. Archibald, S. B. Qadri and B. P. Gaber, *Langmuir*, 1996, **12**, 538.
47 D. B. Wurm, S. T. Brittain and K. Yeon-Taik, *J. Mater. Sci. Lett.*, 1996, **15**, 1285.
48 A. A. Campbell, G. E. Fryxell, G. L. Graff, P. C. Rieke and B. J. Tarasevich, *Scanning Micros.*, 1993, **7**, 423.
49 F. C. Meldrum, J. Flath and W. Knoll, *Thin Solid Films*, 1999, in the press.
50 Y. Golan, L. Margulis and I. Rubinstein, *Surf. Sci.*, 1992, **264**, 312.
51 Y. Golan, L. Margulis, I. Rubinstein and G. Hodes, *Langmuir*, 1992, **8**, 749.
52 C. D. Bain, E. B. Troughton, Y. T. Tao, J. Evall, G. M. Whitesides and R. G. Nuzzo, *J. Am. Chem. Soc.*, 1989, **111**, 321.
53 J. Habitch, PhD Thesis, MPI-Polymerforschung, Mainz, 1998.
54 W. Knoll, *MRS Bull.*, 1991, **16**, 29.
55 H. Raether, *Surface Plasmons on Smooth and Rough Surfaces and on Gratings*, Springer Tracts on Modern Physics, Springer, Berlin, 1998, vol. 111.
56 E. Burstein, W. P. Chen, Y. J. Chen and A. Hartstein, *J. Vac. Sci. Technol.*, 1974, **11**, 1004.
57 T. T. Ehler, N. Malmberg and L. J. Noe, *J. Phys. Chem. B*, 1997, **101**, 1268.
58 J. Spinke, M. Liley, F. J. Schmitt, H. J. Guder, L. Angermaier and W. Knoll, *J. Chem. Phys.*, 1993, **99**, 7012.
59 K. A. Peterlinz and Georgiadis, *Langmuir*, 1996, **12**, 4731.
60 O. Söhnel and J. W. Mullin, *J. Colloid Interface Sci.*, 1988, **123**, 43.
61 J. W. Mullin, *Crystallization*, Butterworth-Heinemann, Oxford, 1993.
62 S. Toschev, in *Crystal Growth: An Introduction*, ed. P. Hartman, North Holland Publishing Company, Amsterdam, 1973.
63 M. C. van der Leeden, D. Verdoes, D. Kashchiev and G. M. van Rosmalen, in *Advances in Industrial Crystallization,* eds. J. Garside, R. J. Davey and A. G. Jones, Butterworth-Heinemann, Oxford, 1991.
64 H. P. Klug and L. E. Alexander, *X-Ray Diffraction Procedures for Polycrystalline and Amorphous Materials*, Wiley, New York, 1976, p. 709.
65 M. K. Norr, *J. Phys. Chem.*, 1961, **65**, 1278.
66 H. Rahnamai, H. J. Gray and J. N. Zemel, *Thin Solid Films*, 1980**,** **69**, 347.
67 N. C. Sharma, D. K. Pandya, H. K. Sehgal and K. L. Chopra, *Thin Solid Films*, 1979, **59**, 157.
68 J. L. Davis and M. K. Norr, *J. Appl. Phys.*, 1966, **37**, 1670.
69 M. J. Lochhead, S. R. Letellier and V. Vogel, *J. Phys. Chem. B*, 1997, **101**, 10821.
70 J. Li, K. S. Liang, G. Scoles and A. Ulman, *Langmuir*, 1995, **11**, 4418.
71 R. Popovitz-Biro, J. L. Wang, J. Majewski, E. Shavit, L. Leiserowitz and M. Lahav, *J. Am. Chem. Soc.*, 1994, **116**, 1179.
72 J. Wang, F. Leveiller, D. Jacquemain, K. Kjaer, J. Als-Nielsen, M. Lahav and L. Leiserowitz, *J. Am. Chem. Soc.*, 1994, **116**, 1192.
73 J. H. Fendler and F. C. Meldrum, *Adv. Mater.*, 1995, **7**, 607.
74 B. R. Heywood and S. Mann, *Adv. Mater.*, 1992, **4**, 278.

Paper 8/07100D